Peptide Ligands of pp60^{c-src} SH2 Domains: A Thermodynamic and Structural Study

Paul S. Charifson,*,‡ Lisa M. Shewchuk,‡ Warren Rocque,§ Conrad W. Hummel,||,⊥ Steven R. Jordan,‡,# Christopher Mohr,‡ Gregory J. Pacofsky,|| Michael R. Peel,|| Marc Rodriguez,||,○ Daniel D. Sternbach,|| and Thomas G. Consler§

Departments of Structural Chemistry, Protein Biochemistry, and Medicinal Chemistry, Glaxo Wellcome, Inc., Five Moore Drive, Research Triangle Park, North Carolina 27709

Received January 2, 1997⊗

ABSTRACT: Thermodynamic measurements, structural determinations, and molecular computations were applied to a series of peptide ligands of the pp60^{c-src} SH2 domain in an attempt to understand the critical binding determinants for this class of molecules. Isothermal titration calorimetry (ITC) measurements were combined with structural data derived from X-ray crystallographic studies on 12 peptide−SH2 domain complexes. The peptide ligands studied fall into two general classes: (1) dipeptides of the general framework *N*-acetylphosphotyrosine (or phosphotyrosine replacement)-Glu or methionine (or S-methylcysteine)-X, where X represents a hydrophobic amine, and (2) tetra- or pentapeptides of the general framework *N*-acetylphosphotyrosine-Glu-Glu-Ile-X, where X represents either Glu, Gln, or NH_2. Dipeptide analogs which featured X as either hexanolamine or heptanolamine were able to pick up new hydrogen bonds involving their hydroxyl groups within a predominantly lipophilic surface cavity. However, due to internal strain as well as the solvent accessibility of the new hydrogen bonds formed, no net increase in binding affinity was observed. Phosphatase-resistant benzylmalonate and α,α-difluorobenzyl phosphonate analogs of phosphotyrosine retained some binding affinity for the pp60^{c-src} SH2 domain but caused local structural perturbations in the phosphotyrosine-binding site. In the case where a reversible covalent thiohemiacetal was formed between a formylated phosphotyrosine analog and the thiol side chain of Cys-188, ΔS was 25.6 cal/(mol K) lower than for the nonformylated phosphotyrosine parent. Normal mode calculations show that the dramatic decrease in entropy observed for the covalent thiohemiacetal complex is due to the inability of the phosphotyrosine moiety to transform lost rotational and translational degrees of freedom into new vibrational modes.

A complete understanding of the forces which mediate the binding of one molecule to another has been elusive. The rapid expansion of structural databases has allowed us "snapshot-based" retrospective analyses of complexation events but leaves some questions unresolved. Given a set of small molecules which associate with the same binding site on the same protein target, several enthalpic and entropic factors are clearly important. Foremost among these are desolvation of both the small molecule and protein, counterion release, loss of rotational and translational degrees of freedom of the small molecule, creation of new vibrational degrees of freedom (largely due to recovery of lost rotational and translational degrees of freedom), conformational changes in the protein induced by the proximal small molecule, and conformational changes in the small molecule induced during complexation with the protein.

Thermodynamic measurements performed in conjunction with structural studies will provide deeper insights into complexation events. Access to both thermodynamic and structural data is becoming more readily available, although the accumulation of thermodynamic information has been slow relative to the ability to obtain structural information. Even with the combination of thermodynamic and structural information, kinetically driven events can never be fully characterized. Examples of structural studies of SH2[1] domains (Waksman et al., 1992, 1993; Gilmer et al., 1994; Overduin et al., 1992; Booker et al., 1992; Eck et al., 1993, 1994; Lee et al., 1994; Pascal et al., 1994; Hatada et al., 1995; Xu et al., 1995) or ITC studies of peptides bound to SH2 domains [p56^{lck} SH2 domain (Lemmon & Ladbury, 1994; Ladbury et al., 1995); pp60^{c-src} and the p85 N-terminal domain of PDGFR (Ladbury et al., 1995)] have been performed in isolation; however, there have been no studies performed on identical complexes of pp60^{c-src} using both

* Address correspondence to this author. Email: psc11602@glaxo.com.
‡ Department of Structural Chemistry.
§ Department of Protein Biochemistry.
|| Department of Medicinal Chemistry.
⊥ Present address: Amgen Boulder Inc., Mail Drop AB/4A, 3200 Walnut Dr., Boulder, CO.
Present address: Amgen, Mail Stop 14-2B, 1840 Dehavilland Dr., Thousand Oaks, CA 91320.
○ Present address: NEOSYSTEM, 7 Rue de Boulogne, 67100 Strasbourg, France.
⊗ Abstract published in *Advance ACS Abstracts,* May 1, 1997.

[1] Abbreviations: DTT, 1,4-dithio-DL-threitol; EDTA, ethylenediaminetetraacetic acid; eu, entropy unit [cal/(mol K)]; GB/SA, generalized Born/solvent-accessible surface area; HEPES, 4-(2-hydroxyethyl)-1-piperazineethanesulfonic acid; ITC, isothermal titration calorimetry; MCMM, Monte Carlo multiple minimum; MD, molecular dynamics; MOPS, 4-morpholinepropanesulfonic acid; PDGF, platelet-derived growth factor; PTK, protein tyrosine kinase; SH2, src homology 2; SH3, src homology 3; pY, phosphotyrosine; pY + 1, amino acid position one residue C-terminal to phosphotyrosine.

S0006-2960(97)00019-6 CCC: $14.00

Chart 1

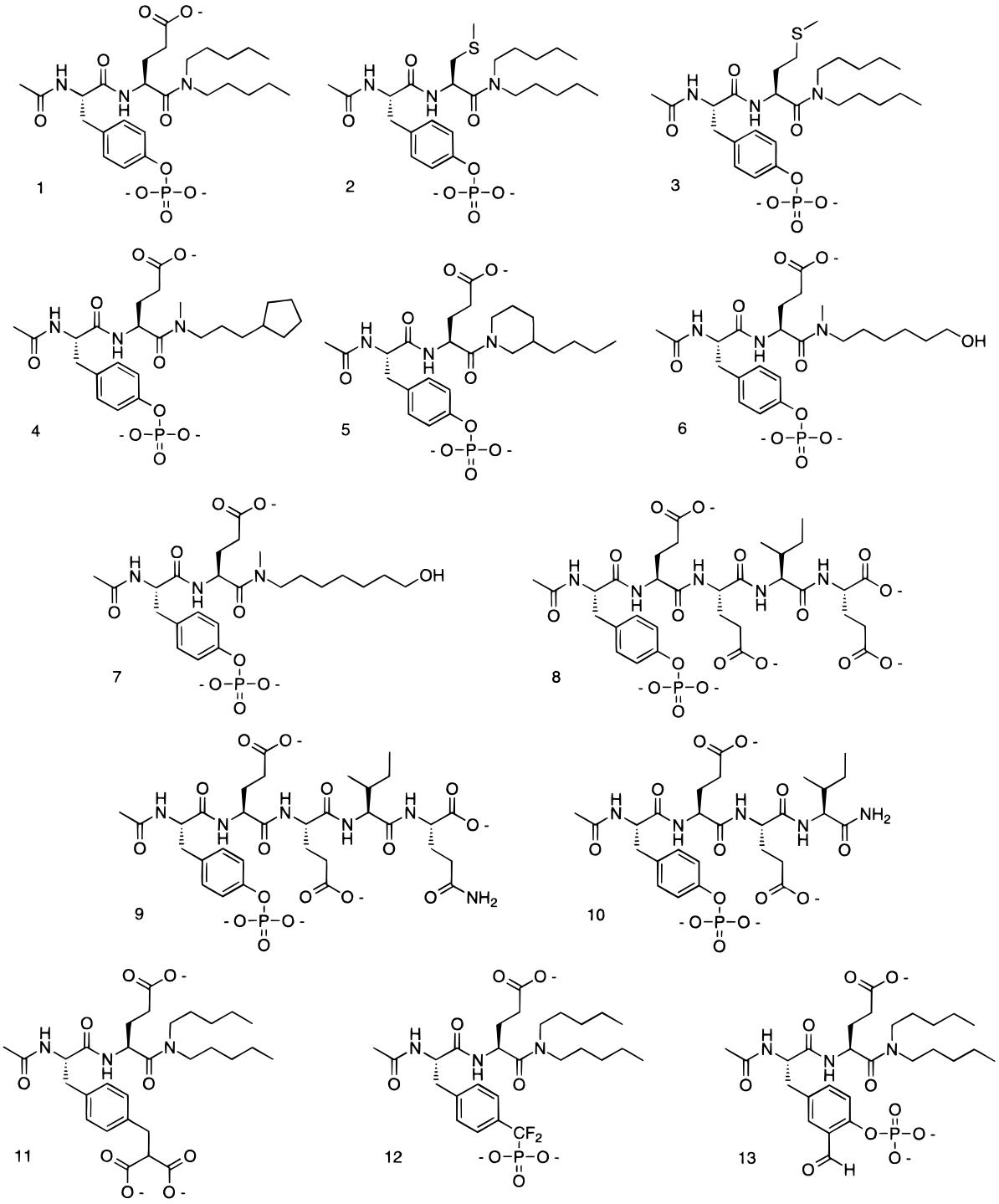

techniques. The concurrent application of thermodynamic and structural techniques has already brought significant insights when applied to other biological systems (Ladbury et al., 1994; Connelly et al., 1994). The present work further illustrates the utility of combining crystallographic and ITC studies on the same system to gain insight into the binding of peptides to the pp60^{c-src} SH2 domain. Interpretation of some of the observed structural and thermodynamic measurements is facilitated by the application of computational chemistry techniques.

Our interest in pp60^{c-src} stems from the involvement of this protein tyrosine kinase (PTK) as a mediator of signal transduction and its role as an intracellular effector for growth factor receptors (Ulrich & Schlessinger, 1990). In its activated form, the protein tyrosine kinase pp60^{c-src} has been implicated in a number of human malignancies including colon carcinoma and breast adenocarcinoma, where association of its SH2 domain with tyrosine-phosphorylated proteins plays a role in pp60^{c-src}-mediated signal transduction. We previously reported a series of peptide inhibitors of pp60^{c-src} SH3−SH2−phosphoprotein interactions (Gilmer et al., 1994). Due to the relative ease of obtaining crystallographic complexes of peptide ligands (Gilmer et al., 1994; Waksman et al., 1992) bound to SH2 domains, this represents an ideal system for accumulating data on several complexes. The compounds considered in this study are shown in Chart 1.

Table 1: Crystallization/Data Collection Conditions

compound	crystallization conditions	data collection temp (°C), cryoprotectant
1	2 M $(NH_4)_2SO_4$, 4 °C	22
2	0.1 M acetate, pH 4.6, 2 M $(NH_4)_2SO_4$, 4 °C	−170, 25% PEG400
3	0.1 M acetate, pH 4.6, 1.5 M $(NH_4)_2SO_4$, 4 °C	4
4	0.1 M acetate, pH 4.6, 2 M $(NH_4)_2SO_4$, 22 °C	22
5	2 M $(NH_4)_2SO_4$, 22 °C	22
6	0.1 M MES, pH 6.5, 0.05 M CsCl, 30% Jeffamine M-600, 4 °C	−170, 25% PEG400
7	0.1 M MES, pH 6.5, 0.2 M $(NH_4)_2SO_4$, 20% PEG2000, 4 °C	−170, 25% PEG400
8	0.1 M acetate, pH 4.6, 10% PEG4000, 22 °C	−170, 25% PEG400
11	2 M $(NH_4)_2SO_4$, 4 °C	4
12	0.1 M acetate, pH 4.6, 2.1 M $(NH_4)_2SO_4$, 4 °C	−170, 10% PEG400, 10% glycerol
13	0.1 M acetate, pH 4.6, 2 M sodium formate, 4 °C	−170, 25% glycerol
13a	1.0 M Li_2SO_4, 2% PEG8000, 4 °C	−170, 25% glycerol

EXPERIMENTAL PROCEDURES

Materials. The expression and purification of all recombinant proteins are described by Gilmer et al. (1994), except for the pp60^{c-src} SH2 C188A mutation, which is described by Boerner et al. (1995).

8−**10** were prepared as described by Gilmer et al. (1994). The synthesis of **1**−**7** and **11**−**13** will be the focus of subsequent papers. All other reagents were commercially available.

Crystallography Methods. Human pp60^{c-src} SH2−ligand crystals were grown by the hanging drop vapor diffusion method. Protein (∼125 mg/mL in 20 mM HEPES, pH 8.0, 350 mM NaCl, 5 mM DTT, and 5 mM EDTA) was mixed with an equal molar ratio of ligand dissolved in an equal volume of reservoir solution, as described in Table 1. For data collected at −170 °C, crystals were soaked in cryoprotectant (Table 1) for 30 min before being frozen in liquid nitrogen. Data were collected on a Rigaku RAXIS IIC area detector mounted on a Siemens rotating anode X-ray generator. Statistics of the data collection are given in Table 2.

The structure of the complex with **8** was solved as described by Gilmer et al. (1994). This protein structure was used as the starting model to solve the complex with **1** by molecular replacement. The remaining structures were subsequently solved using the refined protein structure of the complex with **1** as a starting model. All structures were manually rebuilt using FRODO (Jones, 1985) and refined with X-PLOR (Brunger, 1990). In all cases backbone dihedral angles fall within allowed regions of the Ramachandran plot, and all geometric parameters are equal to or better than average, compared with well-refined structures at comparable resolution, as determined by PROCHECK (Laskowski et al., 1993).

Isothermal Titration Calorimetry Methods. The titration of the pp60^{c-src} SH2 domain with peptide ligands was carried out using a MicroCal MCS titration calorimeter (MicroCal Inc., Northhampton, MA) as described by Wiseman et al. (1989). pp60^{c-src} SH2 was desalted into either 20 mM HEPES and 150 mM NaCl, pH 8.0, or 100 mM sodium acetate and 150 mM NaCl, pH 4.6. Peptide ligands were dissolved in the same buffer as the pp60^{c-src} SH2 protein. The pH of concentrated peptide stock solutions was adjusted by titration with 1.0 M NaOH as needed. In a typical experiment, the peptide ligand (1−3 mM in a 100 μL syringe) was titrated over 15−20 injections of varying volumes (2−10 μL) into purified pp60^{c-src} SH2 (20−50 μM) at 25 °C. Titrations were performed at 3−6 min intervals at a stirring speed of 600 rpm. The quantity of heat released due to peptide ligand binding to pp60^{c-src} SH2 was measured by integrating the area of each titration peak. Data analysis and curve fitting were carried out using the Origin software package supplied by MicroCal. Heats measured during protein−ligand titration experiments were corrected for the heat of dilution of each ligand prior to data analysis. In most cases, this was accomplished by performing separate control experiments wherein ligand solutions were titrated into buffer alone. Alternatively, the heat of dilution of each ligand was subtracted using heats measured after saturation had been obtained during the protein titration experiments. Protein concentrations were determined on a Hewlett-Packard 8452A diode array spectrophotometer using a derived functional extinction coefficient of 0.0156 μM^{-1} cm^{-1}.

pK_a Determinations. The determinations of pK_{a_2} for phenyl phosphate and 2-formylphenyl phosphate were performed by UV spectroscopy. A single solution multicomponent buffer containing 5 mM each of glycine, MOPS, and sodium acetate at 25 °C was used to cover a pH range from 2.2 to 7.8. The solution was initially adjusted to approximately pH 2.2 using 1.0 N HCl. Spectrophotometric titrations were performed at 267 nm for phenyl phosphate and 325 nm for 2-formylphenyl phosphate using 1.0 N NaOH as the titrant. The acid ionization constants were derived from nonlinear regression of the pH vs absorbance data.

Computational Methods. Ab initio calculations were performed using Gaussian 92 (Frisch et al., 1992). Basis sets used for specific calculations are referred to in the Results and Discussion section. Solvation free energies were calculated via the semiempirical AM1-SM2 model using AMSOL (Cramer & Truhlar, 1991, 1992). Monte Carlo multiple minimum (MCMM) conformational search calculations were performed using BatchMin 4.5 (Mohamadi et al., 1990).[2] The AMBER* molecular mechanics force field (McDonald & Still, 1992; Weiner et al., 1984)[3] was employed as was the GB/SA continuum solvation model (Still et al., 1990).

AMBER 4.1 (Pearlman et al., 1995) was used to perform normal mode calculations (nmode) and analyses (nmanal). Molecular dynamics calculations were performed using the SANDER module of AMBER 4.1. All simulations were performed for 500 ps after water equilibration (10 ps) and gradual heating stages (4−6 ps). For the free ligand simulations, constant pressure, periodic boundary solvated dynamics were performed, while for the complexes, an 8.0 Å shell of waters solvated the system. For the nonperiodic simulations of the complexes, an $\epsilon = r$ dielectric model was used to prevent solvent evaporation (Guenot & Kollman, 1992, 1993). A 10 Å nonbonded cutoff was employed during all simulations. For the normal mode and molecular dynamics simulations involving **13**, calculations were per-

[2] BatchMin is part of the MacroModel molecular modeling program.

[3] The AMBER* parameter set is a reparametrization of peptide torsional parameters based upon the original AMBER 1984 parameter set (Weiner et al., 1984).

Table 2: Crystallographic Data

compound	space group	mol/asu[a]	cell dimensions (Å/deg)	resolution (Å)	R_{merge}[b] (%)	*R*-factor[c] (%)
1	$P2_12_12_1$	2	52.5, 67.1, 74.5/90, 90, 90	2.2	6.5	17.4
2	$P2_12_12_1$	2	52.0, 67.7, 75.2/90, 90, 90	2.4	10.7	19.6
3	$P2_12_12_1$	2	51.9, 67.1, 74.6/90, 90, 90	2.5	8.5	19.2
4	$P2_12_12_1$	2	51.7, 66.9, 75.6/90, 90, 90	2.4	6.1	18.6
5	$P2_12_12_1$	2	51.6, 67.2, 75.2/90, 90, 90	2.2	4.4	19.2
6	$P2_12_12_1$	2	41.5, 68.8, 37.6/90, 90, 90	2.5	9.3	22.7
7	$P2_12_12_1$	2	50.8, 119.2, 37.4/90, 90, 90	2.4	6.2	22.6
8	$P2_12_12_1$	1	41.5, 44.9, 75.6/90, 90, 90	2.0	3.8	19.6
11	$P2_12_12_1$	2	52.5, 67.2, 74.5/90, 90, 90	2.2	4.4	19.0
12	$P2_12_12_1$	2	51.9, 67.4, 75.2/90, 90, 90	2.2	6.9	19.0
13	$P2_12_12_1$	2	51.9, 66.0, 74.1/90, 90, 90	2.0	7.1	22.0
13a	$P2_12_12_1$	2	51.4, 65.4, 74.6/90, 90, 90	2.0	6.4	19.7

[a] mol/asu = molecules per asymmetric unit. [b] $R_{merge} = \sum_i|\langle I_i\rangle - I_i|/\sum_i I_i$; $\langle I_i\rangle$ is the weighted average of I_i over all observed symmetry equivalents. [c] *R*-factor $= \sum_h|F_o - F_c|/\sum_h F_o$; F_o and F_c are the observed and calculated structure factor amplitudes of reflection *h*.

Table 3: Isothermal Calorimetry Data[a]

compound	K_d (μM)	ΔH (kcal/mol)	ΔG[b] (kcal/mol)	ΔS[c] [cal/(mol K)]	occluded SA (Å^2)[d]
1	0.4 ± 0.1	−4.3 ± 0.9	−8.9	15.3	417
2	4.2 ± 1.6	−3.9 ± 0.1	−7.4	11.7	429
3	1.4 ± 0.6	−4.3 ± 0.8	−8.1	12.7	442
4	0.4 ± 0.1	−7.1 ± 0.0	−8.8	5.7	448
5	1.0 ± 0.5	−5.4 ± 0.1	−8.4	10.0	473
6	3.4 ± 1.6	−3.2 ± 0.6	−7.6	14.7	398
7	2.3 ± 0.5	−4.6 ± 0.5	−7.8	10.7	561
8	0.05 ± 0.02	−6.8 ± 0.2	−10.1	11.0	446[e]
9	0.09 ± 0.04	−6.2 ± 0.5	−9.8	12.0	NA
10	0.5 ± 0.2	−5.1 ± 1.1	−8.8	12.3	NA
11	11.7 ± 2.1	−6.8 ± 0.6	−6.8	0.0	442
12	2.4 ± 0.7	−5.1 ± 0.2	−7.8	9.0	435
13	0.2 ± 0.0	−12.2 ± 0.1	−9.1	−10.3	481
13a[f]	0.6 ± 0.1	−1.8 ± 0.3	−8.5	22.3	454

[a] All isothermal calorimetry measurements performed at pH 8.0. [b] ΔG calculated from $-RT \ln K_a$. [c] ΔS calculated from $\Delta G = \Delta H - T\Delta S$. [d] Occluded SA is the exposed molecular surface area lost by both binding partners via the formation of the bimolecular complex. This is calculated as the sum of the differences in the molecular surface areas for the complexed and isolated molecules using a probe of radius 1.4 Å and a surface point density of 10. All calculations were performed on crystallographic structures only. [e] The atomic coordinates for the terminal glutamic acid in this pentapeptide were not available due to poor electron density. [f] Compound **13a** measured against the C188A mutant.

formed on both the covalent thiohemiacetal form in the complexes and on the formyl form free in solution. All subsequent analyses were performed over the final 300 ps of the simulation. In the simulation involving the complex of **8** with the pp60^{c-src} SH2 domain, the starting conformation of the C-terminal glutamic acid was determined via a systematic conformational search using the MVP (Lambert, 1997) program since no clear electron density existed for this residue in the crystallographic complex. Conformational filtering calculations were performed on the final 300 of 500 ps from the molecular dynamics simulations using MVP; in this context, conformational filtering is defined by the exhaustive pairwise rms superposition of all conformer non-hydrogen atoms at a given threshold level. Conformers which differ from all other conformers by the chosen filtering threshold are considered unique.

RESULTS AND DISCUSSION

Toward Understanding SH2 Ligand Peptide Binding. **1** represents the dipeptide ligand standard; the remaining peptides in Table 3 represent a subset of phosphotyrosine (pY), pY + 1, and carboxy-terminal modifications. The mean stoichiometry for binding to the pp60^{c-src} SH2 domain determined from this set of phosphopeptides was found to be 0.97 ± 0.1. The compounds studied possess total molecular charge in the range of −2 to −6 and are expected to possess large desolvation free energies.

Inspection of the crystallographic complex of **1** (Figure 1A) illustrates that the phosphotyrosine binding interactions are identical to those described by Gilmer et al. (1994) and Waksman et al. (1992, 1993). The remainder of the phosphotyrosine-containing molecules in this study all bind quite similarly although analysis of all members of all asymmetric units reveals some subtleties in the orientation of the phosphotyrosine ring in the pY binding site. There are also some variations in the orientation of the phosphate with respect to the guanidinium moiety of Arg-178. Figure 1B illustrates the hydrogen bond formed between the pY + 1 backbone nitrogen of **1** and the carbonyl oxygen of His-204. This hydrogen bond is present in complexes of all compounds included in this study. Figure 1B further shows that, for **1**, one of the two pentyl chains is facing a predominantly lipophilic, yet shallow surface cavity (pY + 3 in the context of formal peptide nomenclature), while the other chain faces solvent. This binding orientation is conserved for all dipentylamide-containing compounds included in this study. It is noteworthy that the first two torsions of the pentyl chain facing the surface are gauche. This conformation is present throughout the dipeptide series and results in a net destabilizing enthalpic contribution of 1.5 kcal/mol. *Ab initio* calculations performed at MP3/6-31G*//MP2/6-31G* show that each gauche torsion incurs 0.75 kcal/mol in conformational strain energy. This agrees with the work of Wiberg and Murcko (1988) and Raghavachari (1984).

pY + 1 Modifications. **2** and **3** were designed with the intent of reducing the total molecular charge from −3 to −2. Since the corresponding aliphatic side chain carbons of Glu at this pY + 1 position pack favorably against the aromatic ring of Tyr-205 (Gilmer et al., 1994; Waksman et al., 1992, 1993), it was thought that the *S*-methylcysteine or methionine side chains would perform a similar role, with the possibility of creating a sulfur−aromatic interaction (Reid et al., 1985) as well. Figure 2A shows that, crystallographically, the *S*-methylcysteine side chain of **2** makes favorable van der Waals interactions with the aromatic ring of Tyr-205 but that a sulfur−aromatic interaction does not occur to any appreciable extent. This is also the case for **3** (Figure 2B). It is encouraging, however, that reducing the total

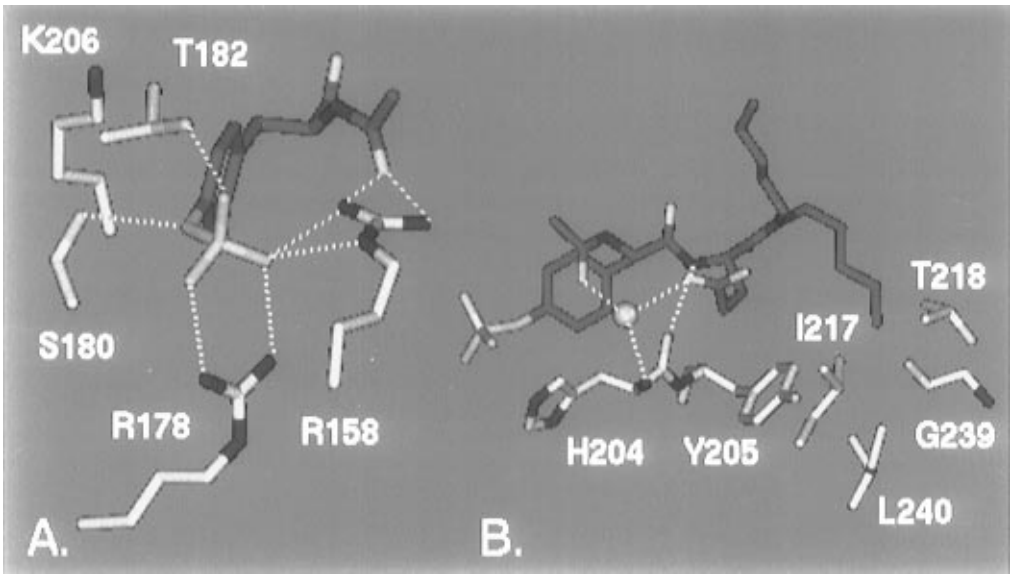

FIGURE 1: **1**, exemplifying the general binding features of phosphodipeptides to the pp60^{c-src} SH2 domain. (A) The phosphotyrosine binding site; hydrogen bonds are denoted by a dotted line. (B) The singular phosphopeptide backbone interaction between the pY + 1 backbone nitrogen of **1** and the His-204 carbonyl oxygen. A highly conserved water molecule is shown bridging **1** to the protein involving the His-204 backbone amide nitrogen. Also shown in this panel is the interaction of one of the pentyl chains with the residues in the lipophilic pocket.

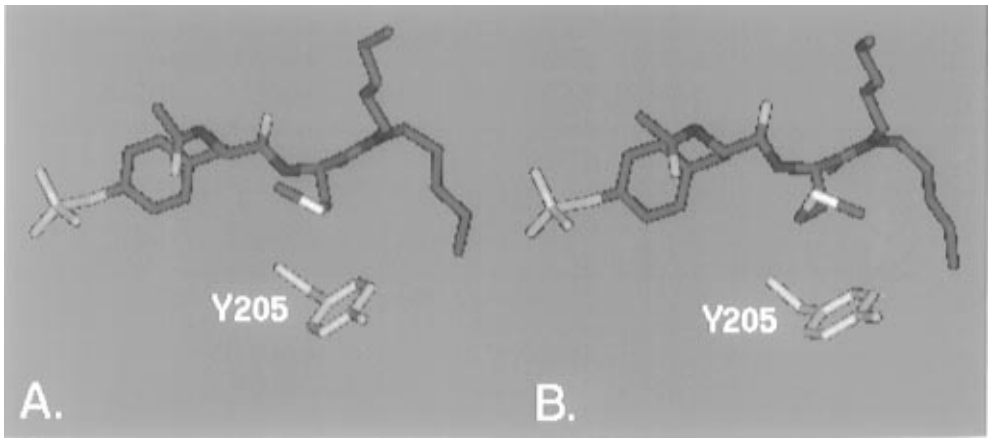

FIGURE 2: Sulfur-containing pY + 1 analogs. (A) The S-methylcysteine side chain of **2** and its proximity to Y205. (B) The methionine side chain of **3** relative to Y205.

charge from −3 to −2 only increased ΔG by 0.8−1.5 kcal/mol relative to **1**. This change in free energy is due to a less favorable entropic contribution for these molecules. This result is difficult to interpret given that we actually observe an increase in occluded surface area when comparing **1** with molecules **2** and **3**. Since more surface area is being buried at the protein−ligand interface, one might expect an increase in entropy according to the generally accepted macroscopic view of the hydrophobic effect. One possible explanation for the less favorable entropic contribution is that the side chains of **2** and **3** more effectively bury their hydrophobicity relative to **1**, thereby restricting the motion of both the ligand and protein partners.

Carboxy-Terminal Modifications. The carboxy termini of these peptides were the most straightforward portion of the molecules in which to make larger structural changes. **4**−**10** provide us with some comparative insights to understand the requirements of the lipophilic binding site. As alluded to above, this site is a shallow cavity usually occupied by hydrophobic residues at pY + 3 (Songyang et al., 1993). The present study builds upon this finding and shows that a variety of hydrophobic groups can bind.

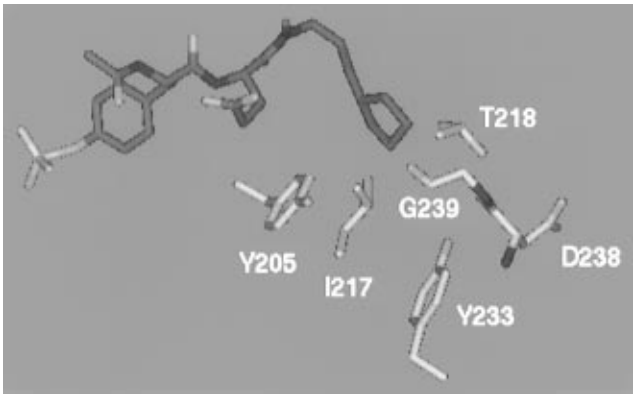

FIGURE 3: The cyclopentyl group of **4** and the residues of the BG and EF loops which define the lipophilic pocket.

(A) Dipeptides. **4** was designed as a cyclic isoleucine analog with the goal of optimizing hydrophobic interactions in the lipophilic site, as well as providing a potential scaffold for later modifications. Analysis of the crystal structure of this complex (Figure 3) and perusal of Table 3 show that an additional 31 Å^2 of exposed surface area is lost upon binding

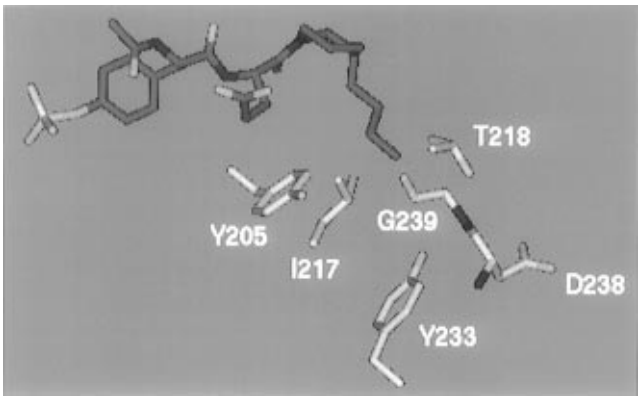

FIGURE 4: Axial orientation of the butylpiperidine portion of **5** at the lipophilic pocket.

relative to **1**; however, the ΔG's for **1** and **4** are equivalent. ΔH is decreased by 3.0 kcal/mol relative to **1**, but ΔS is reduced by 10 eu (entropy units) or 3.0 kcal/mol ($T\Delta S$). These data suggest that a portion of this reduced ΔS results from the restricted motion of the cyclopentyl group in the lipophilic pocket relative to the unbranched alkyl substituent of **1**.

5 represents another attempt to rigidify the carboxy-terminal portion of these molecules. Interestingly, modeling suggested that, in order for this compound to bind to the $pp60^{c-src}$ SH2 domain, the butyl group would adopt an axial orientation with respect to the piperidine ring. The energy cost of this conformation relative to the equatorial conformer is greater by 1.2 kcal/mol (based upon 6-31G* optimizations on axial vs equatorial *N*-acetyl-3-butylpiperidine). The axial preference was borne out crystallographically as illustrated in Figure 4. It is noteworthy that a mixture of diastereomers was used for crystallization trials but only the axial form of one diastereomer was observed in the crystal structure. Electron density corresponding to the equatorial isomer was not observed. The $\Delta\Delta H$ between **5** and **1** represents the stabilization of one to two gauche torsions imposed by this constrained ring system.

In an attempt to maximize hydrophobic contacts while simultaneously establishing a new hydrogen bond, **6** was synthesized. Conformational search calculations performed on the hexanol group predicted that either the Thr-218 side chain oxygen or Gly-239 backbone carbonyl oxygen was a candidate for forming a new hydrogen bond. Figure 5A illustrates that, crystallographically, this alkanol hydrogen bonds to the Thr-218 side chain oxygen. The ΔG of **6** relative to **1** is less favorable by 1.3 kcal/mol; the majority (1.1 kcal/mol) is due to an enthalpic difference. This enthalpic difference is due to the fact that this compound possesses one more gauche interaction than **1**. Although a new hydrogen bond with Thr-218 was formed by this compound, no improvement in overall binding energy was realized.

Similar results are observed with **7**. In this case, the alcohol hydrogen bonds with the backbone carbonyl oxygen of Asp-238 (Figure 5B). This compound shares an equivalent binding affinity with **6**. However, **7** shows a 1.4 kcal/mol more favorable ΔH than **6**, presumably due to greater hydrophobic contact of the heptanol chain in the lipophilic binding site relative to the hexanol chain of **6**. Entropically, **7** experiences a diminution of 4.0 eu relative to **6** due to the loss of one more degree of torsional freedom in going from the unbound to the bound state.

(B) Pentapeptides. **8**−**10** are pentapeptides based on earlier work (Gilmer et al., 1994). Although no direct structural information exists for **9** and **10**, they are sufficiently similar to **8** to draw conclusions from the crystal complex of **8**.

It is interesting that ΔS for **8** relative to **1** is lower by 4.3 eu although the total molecular charge has doubled (−3 for **1** and −6 for **8**). It is not likely that this difference in ΔS is charge driven since **9** (total charge = −5) and **10** (total charge = −4) possess very similar ΔS values with **8**. It is more likely that the degree of overall molecular conformational flexibility is responsible for the differences in ΔS observed between **1** and **8**−**10**.

In an attempt to understand the observed differences in ΔS between **1** and **8**−**10**, conformational filtering calculations were performed at the 0.5 Å threshold level for the ligand non-hydrogen atoms from the molecular dynamics simulations. Although these calculations cannot fully account for observed ΔS differences, they implicitly describe the conformational/configurational entropy contributions. These filtering calculations were performed for both the free and bound states of **1** and **8**. The data from the solution simulations of uncomplexed **1** and **8** show that at the 0.5 Å filtering level there are 229 and 246 unique conformers,

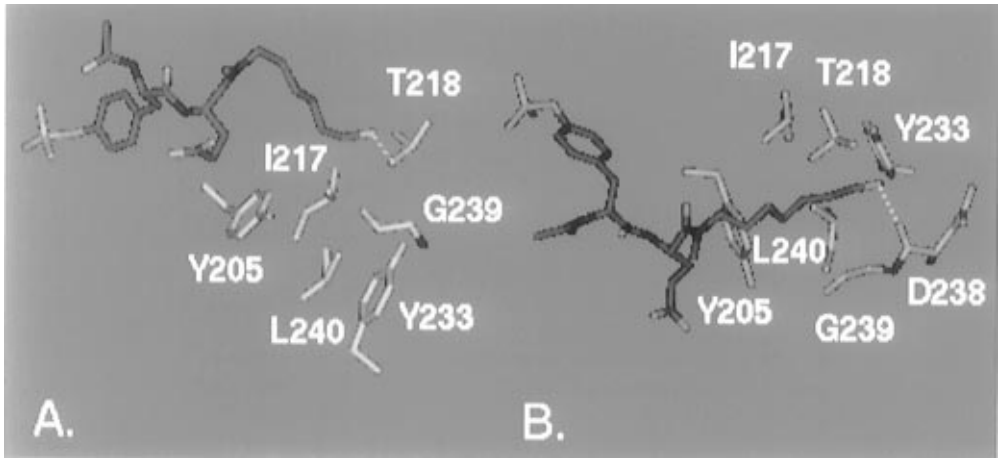

FIGURE 5: (A) Interaction of the hexanol portion of **6** with T218 of the EF loop. The hydrogen bond is designated by a dotted line. The view is rotated slightly from the other figures. (B) Interaction of the heptanol side chain of **7** with the backbone amide carbonyl oxygen of D238. The hydrogen bond is designated by a dotted line. The view is from the top.

respectively, indicating that **8** is more flexible when not complexed with the pp60^{c-src} SH2 domain. However, this trend seems to reverse upon binding. The data from the solution simulations performed on pp60^{c-src} SH2 domain complexes with **1** and **8** show that at the 0.5 Å filtering level there are 14 and 11 unique conformers, respectively. Thus, **8** appears to be less flexible than **1** when bound to the pp60^{c-src} SH2 domain. This may be explained by the fact that the pY + 3 isoleucine of **8** protrudes deeper into the lipophilic surface cavity than does the terminal methyl of the dipentylamide of **1**. **8**−**10** are, in a sense, "rigid" structures when bound to the pp60^{c-src} SH2 domain; the presence of the adjacent glutamic acids contributes to a fully extended conformation due to charge repulsion of the adjacent negative charges and by forming weak electrostatic interactions with basic surface residues (Gilmer et al., 1994; Waksman et al., 1992, 1993). This serves to position the phosphotyrosine and isoleucine at an optimal distance (10.3 Å between Cβ of phosphotyrosine and isoleucine) for both electrostatic and geometric complementarity with the pp60^{c-src} SH2 surface.

8 and presumably **9** and **10** show less favorable ΔS values by ~ 3−4 eu relative to **1** since they lose more entropy upon binding. The fact that **8**−**10** show an overall ΔG more favorable than **1** is accounted for by a better binding enthalpy due to the greater number of charge−charge interactions.

Phosphotyrosine Modifications. (*A*) *Phosphate Replacements.* The phenyl phosphate portion of all SH2 ligands is perhaps the most interesting and challenging group to modify. Ideally, a neutral, phosphatase-resistant mimic would be desirable. Although phosphatase resistance can be imparted relatively easily, the maintenance of binding affinity concurrent with removal of all negative charge has been much more difficult. SH2 domains have evolved to function as anion-binding sites by virtue of a dense array of basic residues which recognize the −2 charged phosphotyrosine. It may be that abolition of all negative charge removes the key recognition element by which these molecules bind. In this study three different phosphotyrosine modifications are considered, **11**−**13**.

Malonates are commonly used to mimic phosphates; therefore, **11** was designed as the benzylmalonate analog of phosphotyrosine. Both the structural and thermodynamic analyses for this compound complexed to the pp60^{c-src} SH2 domain are quite informative. The ΔG for **11** relative to **1** is 2.1 kcal/mol less favorable due entirely to an unfavorable entropic contribution. The benzylmalonate moiety, although desirable because it distributes its negative charge in an efficient manner and its ability to desolvate more readily, possesses three more non-hydrogen atoms than phenyl phosphate and is 21% larger in terms of molecular volume. AMSOL calculations were performed on phenyl phosphate and benzylmalonate which were constrained to their crystallographic conformation via a single torsion angle (either the P−O−C═C torsion for phenyl phosphate or the corresponding C−C−C−C torsion for benzylmalonate). These calculations suggest that the larger benzylmalonate possesses a solvation free energy which is 57.5 kcal/mol less negative than phenyl phosphate (−217.4 vs −274.9 kcal/mol). The protein strives to neutralize its exposed net positive charge in the pY binding site and will accommodate some structural reorganization. This results in a translation of the BC loop (residues Glu-181 through Gly-185) relative to the complex

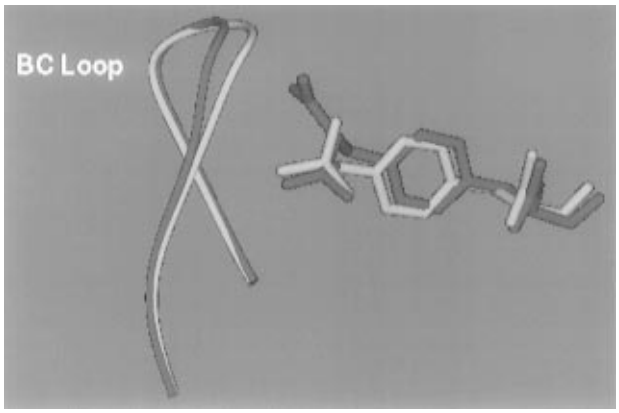

FIGURE 6: Superimposition of the **11** complex and the **1** complex. The *N*-acetylphosphotyrosine portion of **1** and a worm representation of its corresponding protein BC loop are colored red while the *N*-(acetylbenzyl)malonate portion of **11** and a worm representation of its corresponding protein BC loop are colored green. The BC loop in the **11** complex is translated 0.9 Å (backbone atoms; see text) relative to the **1** complex.

Table 4: Effect of pH on Dissociation Constant

	K_d (μM)	
compound	pH 4.6	pH 8.0
1	17.06	0.40
8	2.04	0.05
13	2.19	0.25

with **1** (Figure 6) by 1.3 Å for all non-hydrogen atoms and 0.9 Å for backbone atoms. All protein backbone atoms were used as the basis for superposition, resulting in an overall rmsd of 0.3 Å. Subsequently, the rmsd of either the BC loop non-hydrogen atoms or backbone (Cα, C, N, O) atoms were calculated on the basis of this original superposition. The net effect of this BC loop conformational change induced by the binding of **11** is a greatly reduced ΔS relative to **1**. The BC loop is stabilized by **11**, and there are now fewer available vibrational degrees of freedom. The greater restriction of the larger benzylmalonate group in the pY binding site also contributes to this greatly diminished ΔS. The enthalpic improvement of 2.5 kcal/mol for **11** relative to **1** may be due to the greater ability of the benzylmalonate to present its well-distributed negative charges to the complementary arginines in the phosphotyrosine binding pocket.

Another phosphatase-resistant analog is the α,α-difluorobenzyl phosphonate **12**. It has been determined (Domchek et al., 1992; Burke et al., 1994) that the side chain pK_{a_2} of α,α-difluorobenzyl phosphonate is approximately equivalent to that of phosphotyrosine (~5.7), making **12** a desirable analog for the physiological environment. Three of the compounds studied in this work (**1**, **8**, and **13**) had ITC measurements performed at pH 4.6. For **1** and **8**, there was a significant decrease in K_d (Table 4), relative to the same measurements at pH 8.0 (the reduced effect of pH on **13** is discussed below), which is attributed to a failure to reach pK_{a_2} for the phosphotyrosine. Lemmon and Ladbury (1994) also note a diminution in phosphopeptide binding to the p56^{lck} SH2 domain at pH 5.5 which they attribute to the protonation of the His-180 side chain (equivalent to His-204 in pp60^{c-src}). The protonation state of the phosphate is a more likely explanation for the loss in binding affinity observed at pH 4.6 since the His-204 side chain is not directly involved in ligand binding.

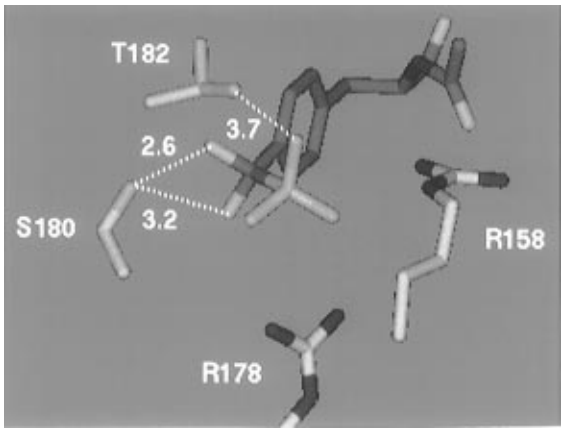

FIGURE 7: Interactions of the difluorophosphonate portion of **12** with the phosphotyrosine binding pocket. The hydrogen bond formed between the *pro-S* fluorine and the side chain hydroxyl of Ser-180 is shown by a dashed line. The distance between the *pro-R* fluorine and Ser-180 is also shown for comparison. The loss of the hydrogen bond formed between one of the difluorophosphonate oxygens and Thr-182 is also denoted by a dashed line.

The use of α,α-difluorobenzyl phosphonate as a pY replacement has been investigated. Burke et al. (1994) reported that hexapeptides containing an α,α-difluorobenzyl phosphonate mimic of phosphotyrosine bound 5-fold more tightly to the pp60^{c-src} SH2 domain than the corresponding phosphotyrosine analogs. Gilmer et al. (1994) previously reported that an α,α-difluorobenzyl phosphonate analog of **8** bound 4-fold less tightly to the pp60^{c-src} SH2 domain. In the present study utilizing ITC data, the α,α-difluorobenzyl phosphonate-containing dipeptide **12** binds 6-fold weaker than its phosphotyrosine-containing dipeptide analog **1** and ∼50-fold less tightly than **8**. Crystallographic complexes of both c-src (Gilmer et al., 1994) and v-src (Waksman et al., 1992, 1993) SH2 domains complexed with phosphorylated peptides show that the phenolic oxygen of phosphotyrosine makes a hydrogen bond with a serine in the conserved FLVRES motif (Figure 1A). Figure 7 shows that, for **12**, the *pro-S* α-fluorine maintains this hydrogen bond with Ser-180; however, the *pro-R* α-fluorine is only weakly involved. In an attempt to estimate the magnitude of the hydrogen bond involving fluorine relative to oxygen, *ab initio* calculations were performed on the methanol dimer vs methanol and 2,2-difluoroethane. The methanol carbon and oxygen atoms of the methanol dimer and both the oxygen and carbon atoms of methanol and both carbon atoms of 2,2-difluoroethane were constrained to the corresponding crystallographic conformations of **1** and **12**, respectively, via a single improper torsional constraint. Calculations were performed at MP2/6-31+G(3df,2p). The resulting $\Delta\Delta E$ shows that the strength of the hydrogen bond involving fluorine is 2.2 kcal/mol weaker than the corresponding hydrogen bond involving oxygen. Although this model system may not be fully reflective of phenyl phosphate vs α,α-difluorobenzyl phosphonate, the trend is likely correct.

A CF_2 group will be approximately 33% larger by volume than an oxygen. This size differential is enough to perturb the interaction with the BC loop by lengthening the hydrogen bond formed between one of the terminal phosphate oxygens and Thr-182. The interaction of the larger CF_2 group of **12** results in the slightly more favorable ΔH relative to **1**. However, ΔG is 1.1 kcal/mol less favorable than **1**, overall. This is due to a less favorable ΔS caused by greater restriction of the larger α,α-difluorobenzyl phosphonate group relative to the phosphate in the phosphotyrosine binding site. Restricted motion, combined with the weaker hydrogen-bonding ability of fluorine relative to oxygen and a weakening of the hydrogen bond involving Thr-182, leads to an overall reduced binding affinity for **12** relative to **1**.

(*B*) *Covalent Modification of Cys-188.* Aside from the issue of phosphatase resistance, the need to improve the overall binding affinity and selectivity of these dipeptides was viewed as a key concern. Inspection of a published sequence alignment of selected SH2 domains (Kuriyan & Cowburn, 1993) shows that, for pp60^{c-src}, the eighth residue downstream from the FLVRES motif is a cysteine (Cys-188) which appears to be unique among the other SH2 domains considered. Although some of the other SH2 domains possess a serine or a threonine at this position, these residues are not as nucleophilic as cysteine. When this observation was viewed in the context of the structural information, some interesting suggestions arose. Analysis of several published crystallographic complexes (Gilmer et al., 1994; Waksman et al., 1992, 1993), as well as those included in this work, showed that the sulfur of Cys-188 was consistently within 3.2−4.0 Å of one of the phosphotyrosine ring meta positions. Placement of a reasonably small electrophilic group at this position could act as a trap for the Cys-188 side chain sulfur. Other investigators have successfully used aldehydes to reversibly trap active site thiols in papain (Westerik & Wolfenden, 1972; Lewis & Wolfenden, 1977) and thymidylate synthase (Chen et al., 1989; Santi et al., 1993). **13**, which possesses a formyl group ortho to the phosphate, was designed to test this hypothesis.

Comparison of K_d values from Table 3 shows that **13** is only slightly better than **1** in its ability to bind to the pp60^{c-src} SH2 domain. One might expect that formation of even a reversible covalent bond would result in a significant net gain in binding affinity. Crystallographically, a covalent thiohemiacetal resulting from the nucleophilic attack of Cys-188 on the formyl group of **13** is observed (Figure 8A). Interestingly, when **13** is bound to the SH2 domain of pp60^{c-src} in which Cys-188 has been mutated to an alanine (i.e., Table 3, **13a**), ΔG is only 0.6 kcal/mol less favorable than when **13** was complexed with the native protein. The crystal complex of this C188A mutant (Figure 8B) shows that the formyl group of **13** is accommodated in the phosphotyrosine binding pocket and is oriented downward near Ala-188. The fact that no covalent adduct with Ala-188 is possible is reflected by a increased ΔH of 10.4 kcal/mol for **13a** relative to **13**.

The effect of pH on the K_d for **13** was less than that for **1** and **8** (Table 4) presumably because formation of a covalent bond reduces the role of the phosphate−arginine interactions in maintaining binding. In the present study, pK_{a_2} for phenyl phosphate was determined to be 6.0 while that for 2-formylphenyl phosphate was found to be 5.4. Although the vast majority of both phenyl phosphate and 2-formylphenyl phosphate would possess a charge of −1 in solution at pH 4.6, the ability of the formylated analog to act as an electrophile for Cys-188 would still be possible at both pHs studied.

Why is this covalent bond formed for **13** worth no more than its noncovalent parent, **1**? Examination of the thermodynamic components of binding provides some insights to this question. Clearly, in enthalpic terms, a ΔH of 8.0 kcal/

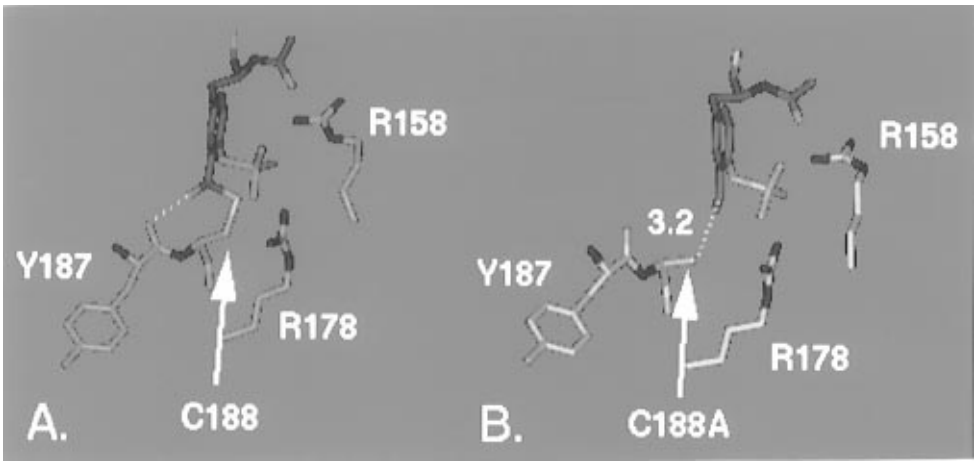

FIGURE 8: (A) Covalent thiohemiacetal complex formed between **13** and C188. The hydrogen bond formed between Tyr-187 and the hydroxyl group of the thiohemiacetal is shown by the dashed line. (B) **13** bound to the pp60^{c-src} C188A mutant (referred to as **13a** in Table 3). The distance between the aldehyde carbonyl carbon and the side chain methyl carbon of Ala-188 is shown by the dashed line.

mol favoring **13** relative to **1** indicates that the covalent thiohemiacetal exists a significant amount of the time. However, entropically, **13** is 25.6 eu less favorable than **1**. Both compounds possess the same net charge (−3), and although some subtle desolvation differences may exist between the two compounds, this could hardly account for this large entropy differential. From analysis of multiple crystallographic complexes spanning several space groups for these dipeptides bound to the pp60^{c-src} SH2 domain, we know that alternate conformations for both the Cys-188 and phosphotyrosine side chains can exist, indicating that there is a certain amount of motion in the phosphotyrosine binding site. A simple interpretation of the dramatically reduced entropy of **13** relative to **1** might be that, in the covalent state, the phosphotyrosine/Cys-188 mobility is restricted, thereby removing degrees of freedom. Additionally, there is a new hydrogen bond formed between the hydroxyl group of the thiohemiacetal and the backbone carbonyl of Tyr-187 (Figure 8A). Further comparison of the crystal complexes of **1** and **13** does not, in fact, give any deeper insights into an entropic term decomposition. The mean temperature factor for the non-hydrogen atoms of residues interacting with the ligands (i.e., residues 158, 178, 180−182, 188, 203−206, 218, 239) is 12.5 Å^2 for **1** and 19.5 Å^2 for **13**. If the protein backbone atoms for the complex with **13** are superimposed upon the same atoms for the complex with **1**, an overall rmsd of 0.5 Å is obtained. Based on this superposition, if the rmsd for only the residues referred to above is measured, the value obtained is 0.5 Å. This indicates that there is no significant difference in the protein conformation in the vicinity of the binding region even though one possesses a covalent bond and the other does not. The conformations of the ligands are also virtually identical; the rmsd for the ligand non-hydrogen atoms based upon the protein superposition above is also 0.5 Å.

One possible explanation for the large entropic difference between **1** and **13** may center around differences in vibrational entropy. In a paper addressing the contribution of vibrational entropy to the dimerization of insulin, Tidor and Karplus (1994) eloquently described how, upon complex formation, the lost translational and rotational degrees of freedom are "recovered" by the formation of six new vibrational modes. On the basis of normal mode analyses they concluded that the dimerization process is responsible for an increase in the vibrational entropy component by 23 eu relative to the two separate monomers. In the present study, normal mode calculations were performed on the **1** and **13** complexes as well as on the free ligands. ΔS's were calculated for each compound in its bound and free states, and then the $\Delta\Delta S$ between the two systems was compared. The calculated vibrational entropy difference between **1** and **13** is −26.5 eu compared with the total experimental $\Delta\Delta S$ of −25.6 eu, suggesting that the favorable vibrational entropy that is recovered upon **1** binding was not achieved by the covalently bound **13**. Further analysis of the normal mode calculations indicates that the torsion angle defined by the central Cβ−Cγ bond of the phosphotyrosine side chain experiences the largest variance between the free and bound states for **13** but not for **1**. The difference in the vibrational intensities between the free and bound states is greatest for this torsion in **13** and is significantly lower for **1**. This Cβ−Cγ torsion would be expected to have a large influence on the overall vibrational oscillations of the phosphotyrosine ring as well as on the phosphate itself. Molecular dynamics calculations incorporating explicit solvent molecules largely support this interpretation. Simulations were performed on **1** and **13** in both the free and bound states, and the ligand torsions were monitored. Analysis of these simulations indicates that the torsion angle defined by the central Cβ−Cγ bond of the phosphotyrosine side chain experiences the largest decrease in motion in going from the free to bound states for **13**. This torsion retains the majority of its rotational range when **1** becomes bound. Since the contribution of the phenyl phosphate to the overall binding affinity is the largest single contribution for any of these ligand molecules, it is likely that the new constraints imposed upon **13** will have a dramatic effect. Although we cannot rule out the possibility that kinetic aspects of reversible thiohemiacetal formation are responsible to a large extent for the net binding profile of **13**, we believe that this thermodynamic interpretation of the observed entropic effects is feasible.

CONCLUSIONS

When ligands intended to bind to macromolecules are designed, the following criteria are generally considered: the formation of new hydrogen bonds, maximization of contact between hydrophobic moieties, stabilization of strained molecular fragments, rigidification, removal of formal charge,

and possibly even the formation of covalent bonds. The combination of isothermal titration calorimetry, X-ray crystallography, and computational analysis applied to a series of peptide ligands of the pp60^{c-src} SH2 domain allows us to evaluate the relative utility of these criteria on ligand design. Thus, designing ligands of SH2 domains serves as a general paradigm for the design of agents to disrupt protein−protein interactions. This work also illustrates some of the difficulties associated with the prediction of ligand binding at shallow exposed protein-binding sites. Although some of the computational methods used in this study were able to correctly predict or explain some of the conformational aspects of ligand binding to the pp60^{c-src} SH2 domain, the magnitude of these interactions was often over- or underestimated. The observed changes in protein conformation upon binding of several of the ligands would have been quite difficult to predict.

Membrane permeability dictates that removal of formal charge from ligand molecules is desirable. Two pp60^{c-src} SH2 ligands with a net charge of −2 were identified in this study. Previously, we were not able to obtain low micromolar binding affinities with net −1 charged molecules (Gilmer et al., 1994). Reducing charge may allow a molecule to desolvate more readily, but this may only maintain binding if the charge neutralization requirements of the system as a whole are met and if conformational strain is not introduced to the protein.

The increased contact between hydrophobic groups affects the thermodynamics of SH2 ligand binding favorably both enthalpically and entropically and is a positive contributor to binding in most situations; the entropic effects appear to hinge on the degree of desolvation achieved. Obtaining new hydrogen bonds which are solvent exposed has a net neutral effect on binding affinity largely because exchange with solvent is entropically disfavored. The enthalpic consequences of solvent-exposed hydrogen bonds can be understood in the macroscopic sense simply by considering differential dielectrics (i.e., $\epsilon_r = 80$ for exposed hydrogen bonds and about 2−3 for buried ones). Additionally, if strain is incurred in another portion of the molecule in order to allow a new hydrogen bond to occur, any favorable increase in binding affinity is mitigated.

Any structural modifications which can rigidify or reduce the strain in the ligand and allow its ground state to be closer to the necessary binding conformation will affect the overall thermodynamics. Enthalpically, allowing the necessary binding determinants to be properly positioned at low conformational energy cost is desirable. Rigidification also avoids the loss in conformational entropy that accompanies the binding of more flexible analogs. In the case of the protein, conformational change may occur to allow ligand binding and stabilize some local region of the protein's energy surface; however, this distortion may also be entropically disfavored due to reducing the overall number of conformational states available to the protein. Finally, the formation of a reversible covalent complex can have a net neutral effect relative to the noncovalent state by severely limiting the gain in new vibrational entropy which often accompanies ligand binding. This effect can be especially important when the covalent bond formed is directly attached to the molecular fragment which contributes the greatest amount to these new vibrational modes.

ACKNOWLEDGMENT

We thank Pamela A. DeLacy and Derril H. Willard for some of the protein purification work, Doug Minick for the pK_a determinations, and Paul L. Feldman for the synthesis of 2-formylphenyl phosphate. We also thank Michael A. Luther, Nobuko Hamaguchi, and Peter W. Jeffs for helpful discussions and encouragement.

REFERENCES

Boerner, R. J., Consler, T. G., Gampe, R. T., Weigl, D., Willard, D. H., Davis, D. G., Edison, A. M., Loganzo, F., Jr., Kassel, D. B., Xu, R. X., Patel, I. R., Robbins, J. S., Lansing, T., Gilmer, T. M., Luther, M. A., & Knight, W. B. (1995) *Biochemistry 34*, 15351−15358.

Booker, G. W., Breeze, A. L., Downing, A. K., Panayotou, G., Gout, I., Waterfield, M. D., & Campbell, I. D. (1992) *Nature 358*, 684−687.

Brunger, A. T. (1990) *Acta Crystallogr. A46*, 46−57.

Burke, T. R., Smyth, M. S., Otaka, A., Nomizu, M., Roller, P. P., Wolf, G., Case, R., & Shoelson, S. E. (1994) *Biochemistry 33*, 6490−6494.

Chen, S. C., Daron, H. H., & Aull, J. L. (1989) *Int. J. Biochem. 11*, 1217−1221.

Connelly, P. R., Aldape, R. A., Bruzzese, F. J., Chambers, S. P., Fitzgibbon, M. J., Fleming, M. A., Itoh, S., Livingston, D. J., Navia, M. A., Thomson, J. A., & Wilson, K. P. (1994) *Proc. Natl. Acad. Sci. U.S.A. 91*, 1964−1968.

Cramer, C. J., & Truhlar, D. G. (1991) *J. Am. Chem. Soc. 113*, 8305−8311.

Cramer, C. J., & Truhlar, D. G. (1992) *Science 256*, 213−217.

Domchek, S. M., Auger, K. R., Chatterjee, S., Burke, T. R., & Shoelson, S. E. (1992) *Biochemistry 31*, 9865−9870.

Eck, M., Shoelson, S. E., & Harrison, S. C., (1993) *Nature 362*, 87−91.

Eck, M., Atwell, S. K., Shoelson, S. E., & Harrison, S. C. (1994) *Nature 368*, 764−769.

Frisch, M. J., Trucks, G. W., Head-Gordon, M., Gill, P. M. W., Wong, M. W., Foresman, J. B., Johnson, B. G., Schlegel, H. B., Robb, M. A., Replogle, E. S., Gomperts, R., Andres, J. L., Raghavachari, K., Binkley, J. S., Gonzalez, C., Martin, R. L., Fox, D. J., Defrees, D. J., Baker, J., Stewart, J. J. P., & Pople, J. A. (1992) *Gaussian 92, Revision A*, Gaussian, Inc., Pittsburgh, PA.

Gilmer, T., Rodriguez, M., Jordan, S., Crosby, R., Alligood, K., Green, M., Kimery, M., Wagner, C., Kinder, D., Charifson, P., Hassell, A. M., Willard, D., Luther, M., Rusnak, D., Sternbach, D. D., Mehrotra, M., Peel, M., Shampine, L., Davis, R., Robbins, J., Patel, I. R., Kassel, D., Burkhart, W., Moyer, M., Bradshaw, T., & Berman, J. (1994) *J. Biol. Chem. 269*, 31711−31719.

Guenot, J., & Kollman, P. A. (1992) *Protein Sci. 1*, 1185−1205.

Guenot, J., & Kollman, P. A. (1993) *J. Comput. Chem. 14*, 295−311.

Hatada, M. H., Xiaode, L., Laird, E. R., Green, J., Morgenstern, J., Lou, M., Marr, C. S., Phillips, T. B., Ram, M. K., Theriault, K., Zoller, M. J., & Karas, J. L. (1995) *Nature 377*, 32−38.

Jones, A. (1985) *Methods Enzymol. 115*, 157.

Kuriyan, J., & Cowburn, D. (1993) *Curr. Opin. Struct. Biol. 3*, 828−837.

Ladbury, J. E., Wright, J. G., Sturtevant, J. M., & Sigler, P. B. (1994) *J. Mol. Biol. 238*, 669−681.

Ladbury, J. E., Lemmon, M. A., Shou, M., Green, J., Botfield, M. C., & Schlessinger, J. (1995) *Proc. Natl. Acad. Sci. U.S.A. 92*, 3199−3203.

Lambert, M. H. (1997) in *Practical Application of Computer-Aided Drug Design* (Charifson, P. S., Ed.) Marcel Dekker, New York (in press).

Laskowski, R. A., MacArthur, M. W., Moss, D. S., & Thornton, J. M. (1993) *J. Appl. Crystallogr. 26*, 283.

Lee, C.-H., Kominos, D., Jacques, S., Margolis, B., Schlessinger, J., Shoelson, S. E., & Kuriyan, J. (1994) *Structure 2*, 423−438.

Lemmon, M. A., & Ladbury, J. E. (1994) *Biochemistry 33*, 5070−5076.

Lewis, C. A., Jr., & Woldenden, R. (1977) *Biochemistry 16*, 4890−4895.

McDonald, D. Q., & Still, W. C. (1992) *Tetrahedron Lett. 33* (50), 7743−7746.

Mohamadi, F., Richards, N. G. J., Guida, W. C., Liskamp, R., Lipton, M., Caufield, C., Chang, G., Hendrickson, T., & Still, W. C. (1990) *J. Comput. Chem. 11*, 440−467.

Overduin, M., Rios, C. B., Mayer, B. J., Baltimore, D., & Cowburn, D. (1992) *Cell 70*, 697−704.

Pascal, S. M., Singer, A. U., Gish, G., Yamazaki, T., Shoelson, S. E., Pawson, T., Kay, L. E., & Forman-Kay, J. D. (1994) *Cell 77*, 461.

Pearlman, D. A., Case, D. A., Caldwell, J. W., Ross, W. S., Cheatham, T. E., III, Ferguson, D. M., Seibel, G. L., Singh, U. C., Weiner, P. K., & Kollman, P. A. (1995) *AMBER 4.1*, University of California, San Francisco.

Raghavachari, K. (1984) *J. Chem. Phys. 81*, 1383−1388.

Reid, K. S. C., Lindley, P. F., & Thornton, J. M. (1985) *FEBS Lett. 190*, 209−213.

Santi, D. V., Ouyang, T. M., Tan, A. K. Gregory, D. H., Scanlan, T., & Carreras, C. W. (1993) *Biochemistry 32*, 11819−11824.

Songyang, Z., Shoelson, S. E., Chaudhuri, M., Gish, G., Pawson, T., Haser, W. G., King, F., Roberts, T., Ratnofsky, S., Lechleider, R. J., Neel, B. G., Nirge, R. B., Fajardo, J. E., Chou, M. M., Hanafusa, H., Schaffhausen, B., & Cantley, L. (1993) *Cell 72*, 767−778.

Still, W. C., Tempczyk, A., Hawley, R. C., & Hendrickson, T. (1990) *J. Am. Chem. Soc. 112*, 6127−6129.

Tidor, B., & Karplus, M. (1994) *J. Mol. Biol. 238*, 405−414.

Ulrich, A., & Schlessinger, J. (1990) *Cell 61*, 203−212.

Waksman, G., Kominos, D., Robertson, S. C., Pant, N., Baltimore, D., Birge, R. B., Cowburn, D., Hanafusa, H., Mayer, B. J., Overduin, M., Resh, M. D., Rios, C. B., Silverman, L., & Kuriyan, J. (1992) *Nature 358*, 646−653.

Waksman, G., Shoelson, S. E., Pant, N., Cowburn, D., & Kuriyan, J. (1993) *Cell 72*, 779−790.

Weiner, S. J., Kollman, P. A., Case, D. A., Singh, U. C., Ghio, C., Alagona, G., Profeta, S., & Weiner, P. (1984) *J. Am. Chem. Soc. 106*, 765.

Westerik, J. O'C., & Wolfenden, R. (1972) *J. Biol. Chem. 247*, 8195−8197.

Wiberg, K. B., & Murcko, M. A. (1988) *J. Am. Chem. Soc. 110*, 8029−8038.

Wiseman, T., Williston, S., Brandts, J. F., & Lin, L.-N. (1989) *Anal. Biochem. 179*, 131−137.

Xu, R. X., Word, J. M., Davis, D. G., Rink, M. J., Willard, D. H., Jr., & Gampe, R. T., Jr. (1995) *Biochemistry 34*, 2107−2121.

BI970019N